

**ANALYSIS OF THE FLOW FIELD IN STENOSED BIFURCATED ARTERIES
THROUGH A MATHEMATICAL MODEL**

S. CHAKRAVARTY AND S. SEN

Received 9 August, 2005; accepted 24 February, 2006; published 13 September, 2006.

DEPARTMENT OF MATHEMATICS, VISVA-BHARATI UNIVERSITY, SANTINIKETAN 731235, INDIA
santabrata2004@yahoo.co.in

ABSTRACT. The present study is dealt with an appropriate mathematical model of the aortic bifurcation in the presence of constrictions using which the physiological flow field is analyzed. The geometry of the bifurcated arterial segment having constrictions in both the parent and its daughter arterial lumen frequently occurring in the diseased arteries causing malfunction of the cardiovascular system, is formed mathematically with the introduction of appropriate curvatures at the lateral junctions and the flow divider. The flowing blood contained in the stenosed bifurcated artery is treated to be Newtonian and the flow is considered to be two dimensional. The motion of the arterial wall and its effect on local fluid mechanics is not ruled out from the present pursuit. The flow analysis applies the time-dependent, two-dimensional incompressible nonlinear Navier-Stokes equations for Newtonian fluid. The flow field can be obtained primarily following the radial coordinate transformation and using the appropriate boundary conditions and finally adopting a suitable finite difference scheme numerically. The influences of the arterial wall distensibility and the presence of stenosis on the flow field, the flow rate and the wall shear stresses are quantified in order to indicate the susceptibility to atherosclerotic lesions and thereby to validate the applicability of the present theoretical model.

Key words and phrases: Stenosis, Arterial Bifurcation, Navier-Stokes Equation.

2000 Mathematics Subject Classification. Primary 92B05, 76Z05. Secondary 76D05, 76M20.

ISSN (electronic): 1449-5910

© 2006 Austral Internet Publishing. All rights reserved.

The present work is part of the Special Assistance Programme [Grant No. F.510/8/DRS/2004(SAP-I)] sponsored by the University Grants Commission (UGC), New Delhi, India.

1. INTRODUCTION

It is an well-established fact that many arterial diseases leading to the malfunction of the cardiovascular system account for more than 50% of the total number of deaths. Atherosclerosis is one such diseases that affects millions of people worldwide in the form of heart attack and stroke. The root causes contributing to the formation of atherosclerotic lesions have long been investigated but yet the progress in understanding is limited to the present scenario. Usually curvatures and bifurcations of large and medium sized arteries are severely affected by this disease. Quite a good number of investigations revealed that there is a relationship between the genesis and the progression of the disease with the locally irregular flow field occurring in these critical regions. Hemodynamics has long been suspected of being involved in such diseases. According to the modern conception , it is widely accepted that the geometry of an arterial bifurcation plays a significant role in atherosclerosis owing to the fact that most lesions are found in these areas as propounded by Wolf and Werthessen [1]. The fact that the arterial walls in these critical sites are exposed to both high and low shear stresses due to adhesion and depositions of blood platelets and lipids, is also well established in recent times. One of the proposed several hypotheses for the role of hemodynamics in the genesis of atherosclerosis is the occurrence of atherosclerosis closely related to high shear stresses, Fry [2] pointed out that a shear stress of 38 N/m^2 for as short as one hour duration can cause degradation in canine arterial walls. He opined also that a moderately elevated wall shear stress or pressure can increase the permeability of endothelial cells. Depending on the geometry of the bifurcated artery, areas of both high and low fluid shear can develop and such phenomena have been evolved from many more studies (Roach and Smith [3], Zarins et al [4] , Ku et al [5], Glagov et al [6], Friedman [7]) involving shear stress hypothesis. For the purpose of conceptual understanding of the flow phenomena through arterial bifurcation from the physiological point of view relevant to the atherosclerotic lesions, one must have the knowledge of hemodynamics, knowledge of atherosclerosis and the correlation between them. Moreover, under normal physiological conditions the transportation of blood in the circulatory system depends entirely on the pumping action of the heart producing a pulsatile pressure gradient throughout the arterial system. For the purpose of gathering more knowledge about the fluid dynamic factor in atherogenesis, quite a good number of theoretical and experimental studies have been carried out over the last years. The various models and methodologies used in these studies are as diversified as the geometric parameters and hydrodynamic conditions of arterial bifurcations. A comprehensive review concerning the specific domain of research under discussion has been successfully conducted by Lou and Yang [8] . The numerical methods appeared to be of much use in supporting experimental methods and can be explored a variety of cases to determine the flow variables which are often difficult to obtain in experiments. Most of the studies dealing with blood flow through arterial bifurcations have been performed with the assumption that the streaming blood as either a Newtonian or a non-Newtonian fluid depending upon the arterial diameters. But Perktold et al [9] observed from their human carotid bifurcation flow model that the non-Newtonian feature did not fundamentally change the flow pattern in the bifurcation. While a considerable number of numerical studies concerns the flow analysis in different two and three-dimensional carotid bifurcation models under rigid wall idealization, relatively few numerical studies incorporating the wall distensibility have been appeared in the literatures (Perktold et al [10]-[11], Chakravarty et al [12]) in recent times. Although a two-dimensional model bifurcation can not provide three-dimensional information, but fortunately, major atherogenic regions around arterial bifurcations are more concentrated in bifurcation planes coinciding with two-dimensional planes especially in early stages of atherosclerosis [13]. Besides these, the flow behavior in mildly stenosed carotid artery bifurcation was less intensively studied. Van de Vosse et al [14]

computed the velocity field in a two-dimensional model of the carotid artery bifurcation in pulsatile flow. They compared the axial velocity profiles in a mildly stenosed bifurcation and a non-stenosed bifurcation and found that the influence of the geometry variation on the axial velocity profiles and the wall shear stress to be relatively small. However, the situations involving severity of the arterial constriction were not adequately explored to have an understanding of the in vivo situations.

In view of the above mentioned facts, an attempt is made to develop a two dimensional aortic bifurcation model mathematically in the present study in order to analyse the flow field for a better understanding of the flow characteristics in the bifurcation. The improved time dependent geometry of the bifurcated artery is constructed mathematically that takes into account two constrictions —one in the parent aorta and another stenosis in the daughter arterial lumen together with the necessary curvatures at the lateral junctions and the flow divider so as to rule out the possibility of any discontinuity, abnormal shear rates and large flow separation zones or non-existent flow separation zones. The streaming blood contained in the stenosed bifurcated artery is treated as Newtonian and the flow is considered to be two dimensional. The cylindrical coordinate system has been taken for analytical formulation. Special emphasis has been put on the effect of arterial wall motion on local fluid mechanics but not on the stresses and strains in the vascular wall. The nonlinear Navier-Stokes equations governing blood flow together with the equation of continuity are undergone a radial coordinate transformation as an initial step and by means of which the velocity field can be expressed more or less in a tractable form with the use of the appropriate choice of the boundary conditions. Finally, the adoption of the finite difference scheme in the present analysis leads to the quantification of the flow field through large scale numerical computation and the influences of the arterial wall distensibility along with the presence of constriction on the flow field, the flow rate and the wall shear stresses are quantified at the end of the paper through graphical display of the results obtained. These results are interpreted and discussed at length in order to validate the applicability of the model under study in the realm of the mechanics of the flow in aortic bifurcation.

2. FORMULATION OF THE PROBLEM

The stenosed bifurcated arterial model under consideration is assumed to be symmetrical about the trunk axis and straight circular cylinders of finite length. Both the parent aorta and its branch are taken to bear constrictions in their lumen. The streaming blood is treated to be Newtonian with constant viscosity while the vessel wall distensibility has been accounted for through the introduction of the arterial wall motion into the local fluid mechanics but not on the stresses and strains on the vessel wall.

Let (r, θ, z) be the coordinates of the representative material point in the cylindrical polar coordinate system of which the z-axis is taken along the axis of trunk while (r, θ) are taken along the radial and the circumferential directions respectively.

The time dependent geometry (Figure 1) of the stenosed bifurcated artery having a couple of stenoses by taking into account the necessary curvatures at the lateral junctions and the flow divider, is developed mathematically as algebraic functions of various model parameters. The geometry of the outer wall is described mathematically as

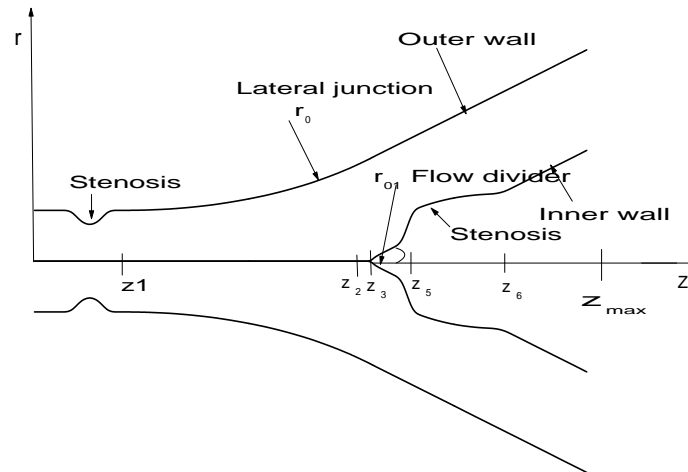


Figure 1: Schematic representation of the stenosed bifurcated artery.

$$(2.1) \quad R_1(z, t) = \begin{cases} a \cdot a_1(t), & 0 \leq z \leq d', d' + l_0 \leq z \leq z_1 \\ \left[a - \frac{4\tau_m}{r_0^2} \{ l_0(z - d') - (z - d')^2 \} \right] \cdot a_1(t), & d' \leq z \leq d' + l_0 \\ \left[a + r_0 - \sqrt{r_0^2 - (z - z_1)^2} \right] a_1(t), & z_1 \leq z \leq z_2 \\ [2r_1 \sec \beta + (z - z_2) \tan \beta] a_1(t), & z_2 \leq z \leq z_{max} \end{cases}$$

while that of the inner wall is given by

$$(2.2) \quad R_2(z, t) = \begin{cases} 0, & 0 \leq z \leq z_3 \\ \sqrt{r_{01}^2 - (z - z_3 - r_{01})^2} b_1(t), & z_3 \leq z \leq z_3 + r_{01}(1 - \sin \beta) \\ (z - z_2) \tan \beta \cdot b_1(t), & z_3 + r_{01}(1 - \sin \beta) \leq z \leq z_5, z_6 \leq z \leq z_{max} \\ \sqrt{r_{02}^2 - (z - z_6)^2} b_1(t), & z_5 \leq z \leq z_6 \end{cases}$$

in which $R_1(z, t)$ and $R_2(z, t)$ represent the respective radii of the outer and the inner wall, a the radius of the parent aorta, r_1 the radius of the branch artery, (r_0, r_{01}) the radii of curvatures for the lateral junction and the flow divider respectively, z_1 the location of the onset of the lateral junction, z_2 the offset of the lateral junction, z_3 the apex, d' the position of the onset of the stenosis in the parent aorta, (z_5, z_6) the respective onset and the offset of the stenosis in the branch artery and β is the semi-bifurcation angle. Here z_{max} has been taken to be the finite length of the arterial segment under consideration. Besides these, the rest of the parameters involved in the above expressions (2.1) and (2.2) should be defined as follows:

$$(2.3) \quad \begin{aligned} a_1(t) &= 1 - (\cos \omega t - 1)k \exp(-k\omega t), \quad b_1(t) = \frac{1}{a_1(t)}, \\ z_2 &= z_1 + \left(\frac{2r_1 \sec \beta - a}{1 - \cos \beta}\right) \sin \beta, \quad z_3 = z_2 + q, \quad r_0 = \frac{2r_1 \sec \beta - 1}{1 - \cos \beta}, \\ r_{01} &= \frac{(z_3 - z_2) \sin \beta}{1 - \sin \beta}, \quad z_6 = z_5 + l \cos \beta, \quad r_{02} = (z_6 - z_2) \tan \beta, \end{aligned}$$

where q is chosen to be a small number lying in the range $0.1 \leq q \leq 0.5$, for compatibility of the geometry, (l_0, l) the respective lengths of the stenoses in the parent and the daughter arteries and k is a constant. Here $\omega = 2\pi f_p$, f_p being the pulse frequency.

Considering the bifurcated arterial blood flow to be nonlinear, axisymmetric, unsteady, two-dimensional, and fully developed with the treatment of a Newtonian fluid representing blood, the usual Navier-Stokes equations and the equation of continuity governing blood flow under pulsatile pressure gradient, may be written as

$$(2.4) \quad \frac{\partial w}{\partial t} + u \frac{\partial w}{\partial r} + w \frac{\partial w}{\partial z} = -\frac{1}{\rho} \frac{\partial p}{\partial z} + \frac{\mu}{\rho} \left(\frac{\partial^2 w}{\partial r^2} + \frac{1}{r} \frac{\partial w}{\partial r} + \frac{\partial^2 w}{\partial z^2} \right)$$

$$(2.5) \quad \frac{\partial u}{\partial t} + u \frac{\partial u}{\partial r} + w \frac{\partial u}{\partial z} = -\frac{1}{\rho} \frac{\partial p}{\partial r} + \frac{\mu}{\rho} \left(\frac{\partial^2 u}{\partial r^2} + \frac{1}{r} \frac{\partial u}{\partial r} - \frac{u}{r^2} + \frac{\partial^2 u}{\partial z^2} \right)$$

and

$$(2.6) \quad \frac{\partial u}{\partial r} + \frac{u}{r} + \frac{\partial w}{\partial z} = 0$$

where $u = u(r, z, t)$ and $w = w(r, z, t)$ are the radial and the axial velocity components of the fluid respectively, p the pressure, ρ the density and μ designates the viscosity of the fluid representing blood.

Further, the pumping action of the heart is idealized by the pulsatile pressure gradient $\frac{\partial p}{\partial z}$ appearing in the axial Navier-Stokes equation (2.4) produced by it, the form of which has been borrowed for humans from Burton [15] as

$$(2.7) \quad -\frac{\partial p}{\partial z} = A_0 + A_1 \cos \omega t, \quad t > 0$$

where A_0 is the constant amplitude of the pressure gradient, A_1 is the amplitude of the pulsatile component giving rise to systolic and diastolic pressure with an angular frequency ω .

3. BOUNDARY CONDITIONS

Along the axis of the artery no radial flow takes place and there is no shear rate of the fluid. This may be expressed mathematically as

$$(3.1) \quad u(r, z, t) = 0, \quad \frac{\partial w(r, z, t)}{\partial r} = 0 \quad \text{on } r = 0, \quad 0 \leq z \leq z_3$$

The velocity field on the outer wall surface may be taken as

$$(3.2) \quad u(r, z, t) = \alpha \frac{\partial R_1}{\partial t}, \quad w(r, z, t) = 0 \quad \text{on } r = R_1(z, t) \quad \text{for all } z,$$

and on the inner half (branch) can be assumed as

$$(3.3) \quad u(r, z, t) = \alpha \frac{\partial R_2}{\partial t}, \quad w(r, z, t) = 0 \quad \text{on } r = R_2(z, t), \quad z \geq z_3$$

in which $\alpha = 1$ for $z < z_3 = \sec \beta$ for $z \geq z_3$.

Moreover, it is assumed that no flow exists when the system is at rest, that means,

$$(3.4) \quad u(r, z, 0) = 0 = w(r, z, 0).$$

4. METHOD OF SOLUTION

To obtain the flow-field of the present theoretical model one may disregard the radial Navier-Stokes equation (2.5) as justified from the assumption of negligible variation of the pressure within the arterial cross section, that is, $p = p(z, t)$ since the arterial radius is relatively much smaller than its finite length. This assumption is well established and supported by several investigators in the past (cf. Womersley [16], Ling and Atabek [17], Imaeda and Goodman [18], Deshpande et al [19] and Pedley [20]).

Since the respective radii $R_i(z, t)$ ($i = 1, 2$) of the outer and the inner wall of the present bifurcated artery are specified by (2.1) and (2.2), the major attention is centered only on the hemodynamic factors.

At the onset of the present analytical treatment, a radial coordinate transformation is initiated with the following substitution

$$(4.1) \quad \xi = \frac{r - R_2(z, t)}{R_1(z, t) - R_2(z, t)} = \frac{r - R_2(z, t)}{R(z, t)},$$

which has the effect of immobilizing the arterial wall in the transformed coordinate ξ . With the introduction of (4.1), the equations (2.4) and (2.6) assume the following form

$$(4.2) \quad \begin{aligned} \frac{\partial w}{\partial t} &= -\frac{1}{\rho} \frac{\partial p}{\partial z} \\ &+ \frac{1}{R} \frac{\partial w}{\partial \xi} \left[\left(\xi \frac{\partial R}{\partial t} + \frac{\partial R_2}{\partial t} \right) + \frac{\mu}{\rho(\xi R + R_2)} \right. \\ &\quad \left. - \frac{\mu}{\rho} \left\{ \frac{\partial^2 R_2}{\partial z^2} + \xi \frac{\partial^2 R}{\partial z^2} - \frac{2}{R} \frac{\partial R}{\partial z} \left(\xi \frac{\partial R}{\partial z} + \frac{\partial R_2}{\partial z} \right) \right\} \right] \\ &+ \frac{\mu}{\rho R^2} \left[1 + \left(\xi \frac{\partial R}{\partial z} + \frac{\partial R_2}{\partial z} \right)^2 \right] \frac{\partial^2 w}{\partial \xi^2} - \frac{u}{R} \frac{\partial w}{\partial \xi} \\ &- w \left[\frac{\partial w}{\partial \xi} - \frac{1}{R} \left(\xi \frac{\partial R}{\partial z} + \frac{\partial R_2}{\partial z} \right) \frac{\partial w}{\partial \xi} \right] + \frac{\mu}{\rho} \frac{\partial^2 w}{\partial z^2} \end{aligned}$$

$$(4.3) \quad \frac{1}{R} \frac{\partial u}{\partial \xi} + \frac{u}{(\xi R + R_2)} + \frac{\partial w}{\partial z} - \frac{1}{R} \frac{\partial w}{\partial \xi} \left(\xi \frac{\partial R}{\partial z} + \frac{\partial R_2}{\partial z} \right) = 0.$$

The accompanied conditions represented by (3.1) - (3.4) should be read according to (4.1) as

$$(4.4) \quad u(\xi, z, t) = 0, \quad \frac{\partial w(\xi, z, t)}{\partial \xi} = 0 \text{ on } \xi = 0 \text{ for } 0 \leq z \leq z_3,$$

$$(4.5) \quad u(\xi, z, t) = \alpha \frac{\partial R_1}{\partial t}, \quad w(\xi, z, t) = 0 \text{ on } \xi = 1 \text{ for all } z,$$

$$(4.6) \quad u(\xi, z, t) = \alpha \frac{\partial R_2}{\partial t}, \quad w(\xi, z, t) = 0 \text{ on } \xi = 0 \text{ for } z \geq z_3$$

and

$$(4.7) \quad u(\xi, z, 0) = 0 = w(\xi, z, 0).$$

Multiplying (4.3) by $(\xi R + R_2)$ and integrating it with respect to ξ , one obtains

$$(4.8) \quad \begin{aligned} u(\xi, z, t) &= \left(\xi \frac{\partial R}{\partial z} + \frac{\partial R_2}{\partial z} \right) w(\xi, z, t) + \frac{R_2}{(\xi R + R_2)} u(0, z, t) \\ &- \frac{R}{(\xi R + R_2)} \int_0^\xi (\xi R + R_2) \frac{\partial w}{\partial z} d\xi \\ &- \frac{1}{(\xi R + R_2)} \int_0^\xi (2\xi R \frac{\partial R}{\partial z} + R_2 \frac{\partial R}{\partial z} + R \frac{\partial R_2}{\partial z}) w d\xi \end{aligned}$$

which subsequently holds the following form subject to the application of (4.5) as

$$(4.9) \quad \begin{aligned} &- \int_0^1 (\xi R + R_2) \frac{\partial w}{\partial z} d\xi \\ &= \int_0^1 \left[(2\xi \frac{\partial R}{\partial z} + \frac{R_2}{R} \frac{\partial R}{\partial z} + \frac{\partial R_2}{\partial z}) w + \frac{R_1}{R} \left\{ \alpha \frac{\partial R_1}{\partial t} - \frac{R_2}{R_1} u(0, z, t) \right\} f(\xi) \right] d\xi. \end{aligned}$$

Since the choice of $f(\xi)$ is arbitrary, one can assume, without any loss of generality, the form of this arbitrary function $f(\xi) = -4\xi(\xi^2 - 1)$ satisfying $\int_0^1 f(\xi) d\xi = 1$.

The equation (4.8) can be rewritten by taking into account the approximation of the treatment of equality between the integrals to integrands together with the condition (4.5) as

$$(4.10) \quad \begin{aligned} u(\xi, z, t) &= \left(\xi \frac{\partial R}{\partial z} + \frac{\partial R_2}{\partial z} \right) w(\xi, z, t) + \frac{R_2}{(\xi R + R_2)} u(0, z, t) \\ &- \frac{\xi^2 R_1}{(\xi R + R_2)} \left\{ \alpha \frac{\partial R_1}{\partial t} - \frac{R_2}{R_1} u(0, z, t) \right\} (2 - \xi^2). \end{aligned}$$

Using (4.10) into (4.2) so that the latter becomes

$$(4.11) \quad \begin{aligned} \frac{\partial w}{\partial t} &= -\frac{1}{\rho} \frac{\partial p}{\partial z} \\ &+ \left[\left(\xi \frac{\partial R}{\partial t} + \frac{\partial R_2}{\partial t} \right) + \frac{\mu}{\rho(\xi R + R_2)} \right. \\ &- \left. \frac{\mu}{\rho} \left\{ \frac{\partial^2 R_2}{\partial z^2} + \xi \frac{\partial^2 R}{\partial z^2} - \frac{2}{R} \frac{\partial R}{\partial z} \left(\xi \frac{\partial R}{\partial z} + \frac{\partial R_2}{\partial z} \right) \right\} \right. \\ &- \left. \frac{R_2}{(\xi R + R_2)} u(0, z, t) - \frac{\xi^2 R_1}{(\xi R + R_2)} \left\{ \alpha \frac{\partial R_1}{\partial t} - \frac{R_2}{R_1} u(0, z, t) \right\} (2 - \xi^2) \right] \frac{1}{R} \frac{\partial w}{\partial \xi} \\ &+ \frac{\mu}{\rho R^2} \left[1 + \left(\xi \frac{\partial R}{\partial z} + \frac{\partial R_2}{\partial z} \right)^2 \right] \frac{\partial^2 w}{\partial \xi^2} + \frac{\mu}{\rho} \frac{\partial^2 w}{\partial z^2} - w \frac{\partial w}{\partial z}. \end{aligned}$$

These equations (4.10) and (4.11) appear to be better representation of the equations governing flow in the bifurcated artery and these would be of some help to obtain the flow field numerically in concert with the boundary conditions without much trouble.

5. FINITE DIFFERENCE APPROXIMATION

The finite difference scheme for discretizing and solving the equations (4.10) and (4.11) numerically is essentially based on the conventional forward difference representation for the time derivative and the central difference formula for the spatial derivatives. The discretized version of the equation (4.11) should now be read as

$$(5.1) \quad w_{i,j}^{k+1} = w_{i,j}^k + \Delta t \left[-\frac{1}{\rho} \left(\frac{\partial p}{\partial z} \right)_i^k + (a_{i,j}^k + b_{i,j}^k + c_{i,j}^k) d_{i,j}^k + e_{i,j}^k + f_{i,j}^k \right],$$

in which the respective expressions for $a_{i,j}^k$, $b_{i,j}^k$, $c_{i,j}^k$, $d_{i,j}^k$, $e_{i,j}^k$ and $f_{i,j}^k$ are included in Appendix for the sake of brevity. The discretization has been performed by defining

$z_i = (i-1)\Delta z$, $i = 1(1)M+1$ and $\xi_j = (j-1)\Delta\xi$, $j = 1(1)N+1$ for the entire arterial segment under consideration where Δz and $\Delta\xi$ represent the respective increments in the axial and the radial directions. Consequently, the discretized version of the boundary conditions (4.4) - (4.7) should be read as

$$(5.2) \quad u_{i,1}^k = 0, \quad w_{i,2}^k = w_{i,1}^k \text{ for } z_i \leq z_3 \text{ and for all } k,$$

$$(5.3) \quad u_{i,N+1}^k = \alpha \frac{\partial R_{1,i}^k}{\partial t}, \quad w_{i,N+1}^k = 0 \text{ for all } z_i,$$

$$(5.4) \quad u_{i,1}^k = \alpha \frac{\partial R_{2,i}^k}{\partial t}, \quad w_{i,1}^k = 0 \text{ for } z_i \geq z_3$$

and

$$(5.5) \quad u_{i,j}^1 = 0 = w_{i,j}^1, \quad i = 1(1)M+1, \quad j = 1(1)N+1.$$

The solutions of (5.1) can be obtained numerically by using the relevant conditions mentioned above. These solutions are then used to determine u from (4.10) directly. Unlike the flow-field in the parent aorta, the velocity components in the branched arteries along the oblique line inclined at an angle β with the parent axis are defined by the following truncated Taylor's series expressions as

$$(5.6) \quad w_{i,j}^{/k} = w_{i,j}^k - \Delta\xi(j-1) \tan\beta \frac{\partial w_{i,j}^k}{\partial z} + \frac{1}{2} [\Delta\xi(j-1) \tan\beta]^2 \frac{\partial^2 w_{i,j}^k}{\partial z^2} + \dots$$

$$(5.7) \quad u_{i,j}^{/k} = u_{i,j}^k - \Delta\xi(j-1) \tan\beta \frac{\partial u_{i,j}^k}{\partial z} + \frac{1}{2} [\Delta\xi(j-1) \tan\beta]^2 \frac{\partial^2 u_{i,j}^k}{\partial z^2} + \dots$$

and consequently their discretized form with first order approximations should be read as

$$(5.8) \quad w_{i,j}^{/k} = w_{i,j}^k - \left(\frac{j-1}{2\Delta z} \right) \Delta\xi \tan\beta (w_{i+1,j}^k - w_{i-1,j}^k) + O(h^2),$$

$$(5.9) \quad u_{i,j}^{/k} = u_{i,j}^k - \left(\frac{j-1}{2\Delta z} \right) \Delta\xi \tan\beta (u_{i+1,j}^k - u_{i-1,j}^k) + O(h^2),$$

h being the width of the mesh.

The volumetric flow rate (Q_p) for the parent ($z < z_3$) aorta and the net flux (Q_d) for the daughter ($z \geq z_3$) arteries can thus be obtained as

$$(5.10) \quad Q_p = 2\pi R_i^k [R_i^k \int_0^1 \xi_j w_{i,j}^k d\xi_j + R_{2,i}^k \int_0^1 w_{i,j}^k d\xi_j],$$

$$(5.11) \quad \begin{aligned} Q_d &= -\pi R_i^k \int_0^{\frac{\sec \beta}{2}} (\xi_j R_i^k + R_{2,i}^k) (w_{i,j}^k \cos \beta + u_{i,j}^k \sin \beta) d\xi_j \\ &+ \pi R_i^k \int_{\frac{\sec \beta}{2}}^1 (\xi_j R_i^k + R_{2,i}^k) (w_{i,j}^k \cos \beta + u_{i,j}^k \sin \beta) d\xi_j. \end{aligned}$$

Finally, the wall shear stresses on the parent outer wall and the daughter inner wall should have the following derived expressions as

$$(5.12) \quad \tau_{out} = \mu \left[\alpha \frac{\partial^2 R_1}{\partial z \partial t} - \frac{1}{R \Delta \xi} \frac{\partial R_1}{\partial z} \left(\alpha \frac{\partial R_1}{\partial t} - u_{i,N}^k \right) - \frac{1}{R \Delta \xi} w_{i,N}^k \right],$$

$$(5.13) \quad \tau_{in} = \mu \left[\alpha \frac{\partial^2 R_2}{\partial z \partial t} - \frac{1}{R \Delta \xi} \frac{\partial R_2}{\partial z} \left(u_{i,2}^k - \alpha \frac{\partial R_2}{\partial t} \right) + \frac{1}{R \Delta \xi} w_{i,2}^k \right].$$

Here the suffixes '*p*', '*d*', '*out*', and '*in*' indicate the parent, the daughter, the outer wall and the inner daughter wall respectively.

6. NUMERICAL RESULTS AND DISCUSSION

The applicability of the present mathematical model is based on the large scale numerical computation of the flow field together with various relevant quantities of interest depending upon the existing data for the physical parameters encountered in the present analysis. An extensive quantitative analysis has been performed with the use of the following data (cf. Milnor[21], Lou and Yang [8]) :

$$\begin{aligned} a &= 11 \text{ mm}, \quad l_0 = 4 \text{ mm}, \quad d' = 4 \text{ mm}, \quad z_1 = 10 \text{ mm}, \quad z_2 = 36 \text{ mm}, \quad z_3 = 36.5 \text{ mm}, \\ z_5 &= 40 \text{ mm}, \quad z_6 = 50.6 \text{ mm}, \quad \tau_m = 0.3a, \quad f_p = 1.2 \text{ Hz}, \quad \beta = 45^\circ, \quad \rho = 1.05 \times 10^3 \text{ Kg m}^{-3}, \\ z_{max} &= 60 \text{ mm}, \quad \mu = 0.035P, \quad r_1 = 0.7a, \quad k = 0.1, \quad A_0 = 10 \text{ Kg m}^{-2} \text{ s}^{-2}, \quad A_1 = 0.2A_0. \end{aligned}$$

The finite difference scheme adopted in the present analysis primarily to solve (5.1) numerically has been found to converge satisfactorily with the respective spacings $\Delta z = 0.1$ and $\Delta \xi = 0.01$ while the time step has been chosen to be $\Delta t = 0.00001$. The necessary convergence of the results has been successfully achieved with the desired degree of accuracy and the results are displayed through the Figs. 2-19 and discussed at length in order to validate the applicability of the present model.

The results of Figure (2) represent the behaviour of the axial velocity profile of the streaming blood in the parent aorta at a specific location of $z = 6 \text{ mm}$ corresponding to the constricted site for three different time periods. The present figure also includes the corresponding results for two more cases at a particular instant of $t=2\text{s}$ — by disregarding the parental constriction in one and by withdrawing the wall motion in another. All the curves appear to be flattened almost half way towards the wall keeping their respective maxima on the axis and then to diminish gradually towards the wall surface to approach minimum value (zero) on the outer surface. One may observe from their behaviour with time that the axial velocity gets enhanced with the advancement of time more towards the axis than in the vicinity of the wall surface.

One may also notice that there is a considerable deviation of the results both with respect to 'nonstenotic' and 'no wall motion' which eventually quantify the effects of stenosis and the distensibility of the arterial wall on the axial velocity profile plotted for the same instant of time. The presence of constriction causes the axial velocity to slow down considerably as one moves away from the wall and similar is the effect of wall motion on the flow profile.

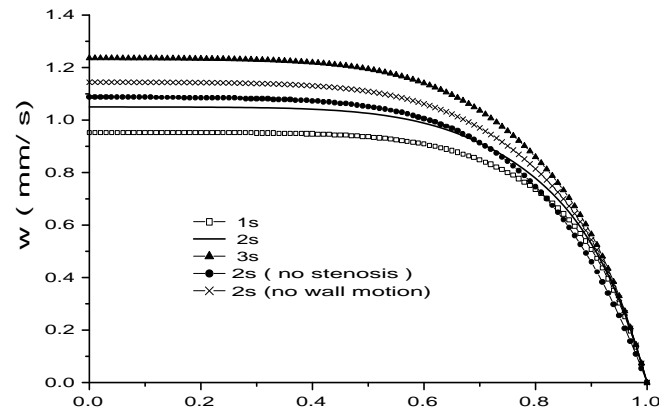


Figure 2: Axial velocity profile for the parent aorta at $z=6$ mm for different time periods.

Unlike the behaviour of the axial velocity profile, the results of the radial velocity component varying radially at the same critical location of $z=6$ mm exhibited in Figure (3) are noted to be alternately negative and positive for three given time periods. Both the bottom most curves corresponding to $t=1$ s and 3 s appear to decline from zero on the axis as one moves away from it and eventually to increase towards the wall to attain some finite values on the wall surface.

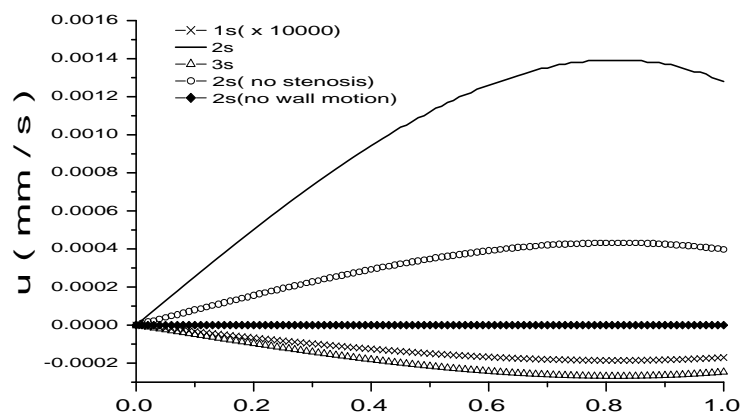


Figure 3: Radial velocity profile for the parent aorta at $z=6$ mm for different time periods.

Conversely, the topmost curves corresponding to $t=2s$ are observed to increase from zero on the axis, rise to definite peaks and then slightly diminish towards the wall surface. From the noted deviation of the results of these two curves one can easily quantify the effect of stenosis on the radial velocity profile. The presence of constriction helps enhancing the radial flow velocity to a large extent unlike the axial velocity presented in Figure 2. Most of the curves of the present figure appear to be concave upwards or downwards in the vicinity of the wall surface excepting that for the rigid vessel (no wall motion) where the profile becomes almost symmetrical. It is again interesting to note that the vascular rigidity reduces the radial velocity of the streaming blood to an extent so that the profile gets shifted towards the origin with zero velocity on the wall surface. The finite non-zero (positive or negative) velocity on the wall surface possesses a reflection of the wall motion encountered in the present model. Although the magnitudes of the radial flow velocity are all time lower than those of the axial velocity, but the effects of parental constriction and the distensibility of the arterial wall are recorded more on the radial velocity profile than on the axial velocity profile of the flowing blood.

Figure (4) shows the results of the axial velocity profile in the daughter arteries at a critical location of $z = z^*$ where the stenosis in the daughter artery assumes its maximum constriction for three different time periods. Two more curves are also plotted in the present figure at a particular instant of $t=2s$ — one by disregarding the presence of constriction while the other by withdrawing the wall motion from the system. All the curves appear to rise from zero on the inner daughter wall, attain their maxima and then gradually diminish to zero on the outer wall surface.

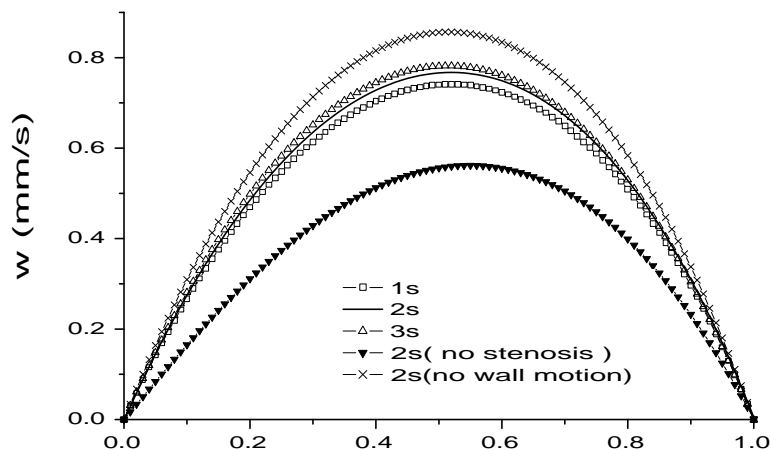


Figure 4: Axial velocity for the daughter artery at $(z = (z_5 + z_6)/2)$ for different times.

There is a drastic change of the axial velocity profile in the daughter artery over that in the parent aorta due to the obvious reasons of the bifurcated flow phenomena where the direction of the flow alters from parent duct to its branches. One may observe that the presence of constriction causes significant increase of the axial velocity in the daughter artery in contrast with that in the parent aorta and such enhanced velocity is recorded maximum towards the mid-way from inner to outer wall surface. So, the effect of stenosis in the daughter arterial lumen

on the axial velocity profile is found to be quite significant. There is also some notable effect of vessel wall distensibility on the velocity profile of the streaming blood in the branched artery.

The unsteady behaviour of the radial velocity profile of the stream in the daughter artery at the same critical location of $z = z^*$ is shown in Figure (5) for three different times. The appearance of negative velocities indicates the back flow right from the inner wall to the outer wall surface. All the curves representing the radial velocities drop from zero on the inner wall surface, attain their minima at a short distance away from the inner wall and then rise to become zero again on the outer wall surface.

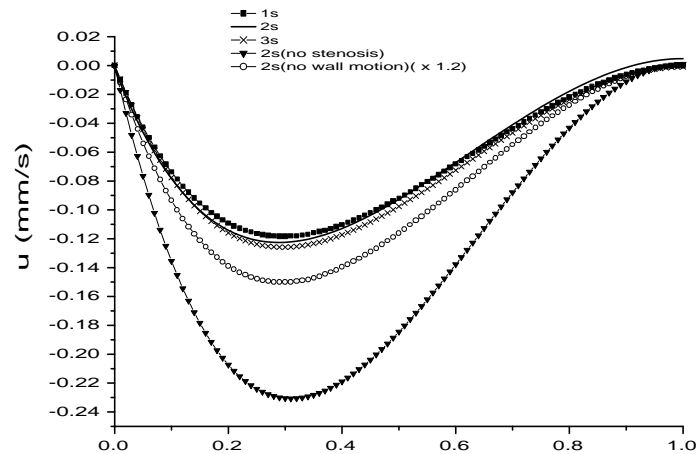


Figure 5: Radial velocity profile for the daughter artery at $z=z^*$ for different times.

The velocity gets diminished further with considerable deviation in magnitude if one disregards the presence of stenosis in the daughter arterial lumen of the present model. When the wall motion is totally withdrawn, that is, for a rigid bifurcated artery, the velocity profile also gets perturbed to some extent more towards the inner wall vicinity than near the outer wall. Thus one can easily quantify the effects of stenosis and the vascular deformability on the radial velocity pattern of the branched artery. It may be of some importance to record that although the magnitudes of the radial velocity are greatly enhanced in the branch artery than those in the main aorta but these are, however, quite smaller than those of the axial velocity in the daughter arteries.

Figures (6) and (7) represent the respective axial and the radial velocity profiles in the daughter arteries at four distinct locations corresponding to a particular instant of $t=2s$. The general features are the occurrence of strongly skewed velocity profiles with positive and negative values in both the directions respectively in the proximal part of the branches with steep velocity gradients at the flow divider walls ($z = z_3$). At the onset ($z = z_5$) of the stenosis, the axial velocity is diminished largely with an almost symmetrical flow pattern about the mid-wall while a reverse flow (from negative to positive values) with smaller magnitudes occurs in the radial direction.

The critical site ($z = z^*$) of the stenosis in the daughter artery, however, experiences enhanced axial velocity from that at the onset and a back flow again along the radial direction.

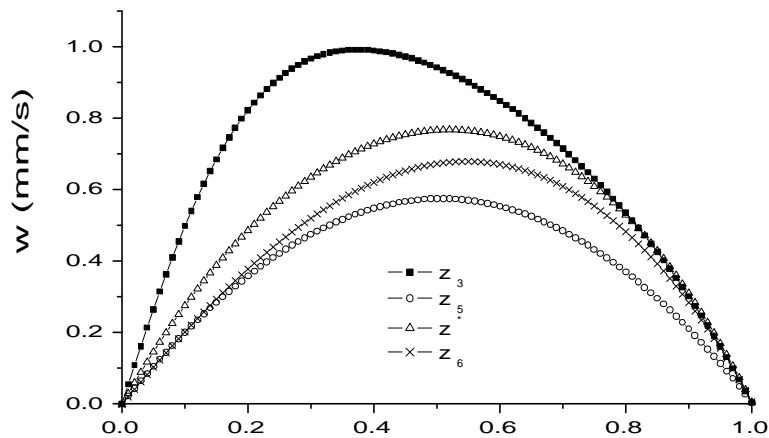


Figure 6: Axial velocity for the daughter artery for different axial positions at $t = 2s$.

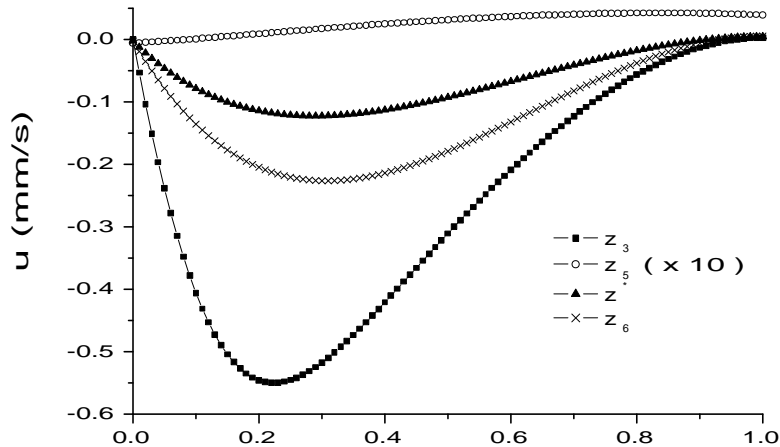


Figure 7: Radial velocity for the daughter artery for different axial positions at $t = 2s$.

Finally, at the offset, that is, distal to the stenosis ($z = z_6$) the axial flow velocity is reduced significantly where the peak velocity is attained more towards the outer wall unlike other patterns but the radial velocity continues to move further backward following the usual pattern. All these observations agree qualitatively well with those of (Perktold and Rappitsch [22]) who studied the flow characteristics of blood through a compliant carotid bifurcation model. One notable feature from the results of the present figures is that both the profiles get largely perturbed near

the apex of all the chosen sites with enhanced magnitudes right from the inner wall vicinity to the area towards the outer wall.

The variations of the flow rate with time spanned over quite a few cardiac cycles within a period of 10s at the apex are exhibited in Figure (8) for three different cases — first based on the present updated model, the second having no wall motion and the third in the absence of constriction. The flow rate appears to get accelerated in the systolic phase and decelerated in the diastolic phase of the first cardiac cycle followed by similar fluctuations with gradually diminishing amplitudes for a few more cardiac cycles in succession and finally these fluctuations completely damp out for the rest of the time.

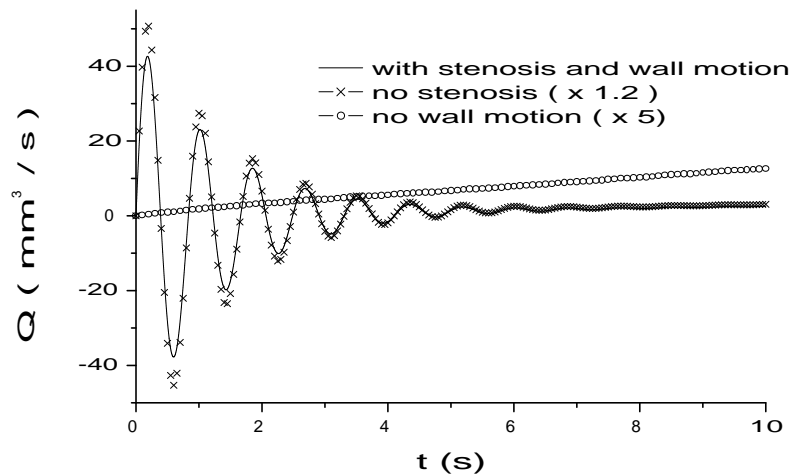


Figure 8: Variation of the flow rate with time at the apex.

One may notice from the behaviour of the flow rate that back flow does occur and several flow separation zones are formed as the direction of the flow rate changes from positive to negative, negative to positive and so on during the period of nearly six cardiac cycles. In the absence of the stenosis, the flow rate follows the analogous trend with a little reduction of magnitudes for the entire time range considered here. So, there is no significant effect of constriction noted on the flow rate at the apex. If one disregards the wall motion, the flow rate behaviour changes drastically to show an all time increasing trend with much reduced magnitudes where no back flow takes place. Thus the vessel wall distensibility helps reducing the flow rate to a considerable extent and its effect can easily be quantified through a direct comparison of the relevant curves of the present figure. The subsequent figures (9) (10) (11) exhibit almost analogous behaviour of the flow rate excepting some deviations in magnitudes at three respective specific locations— one at the onset of the stenosis, other at the maximum constriction site of the stenosis and finally at the offset of the stenosis of the daughter artery.

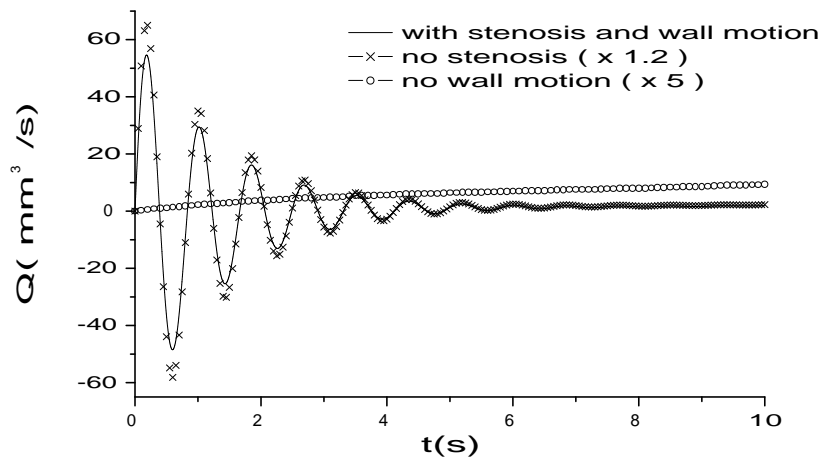


Figure 9: Variation of the flow rate with time at the onset of the stenosis.

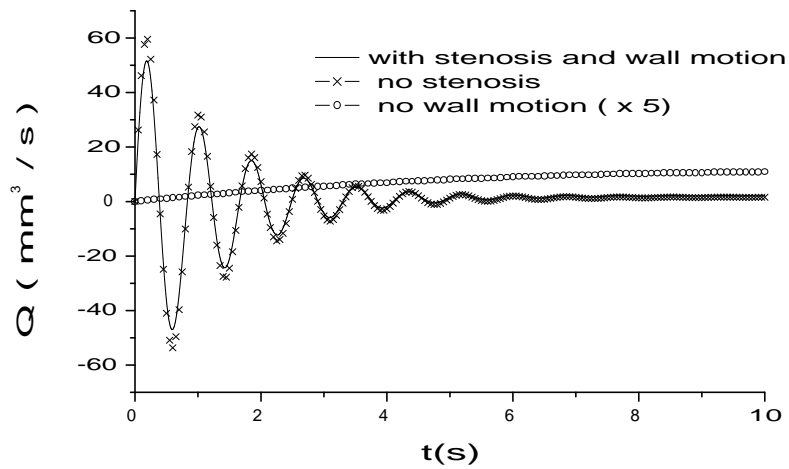


Figure 10: Variation of the flow rate with time at the maximum constriction site.

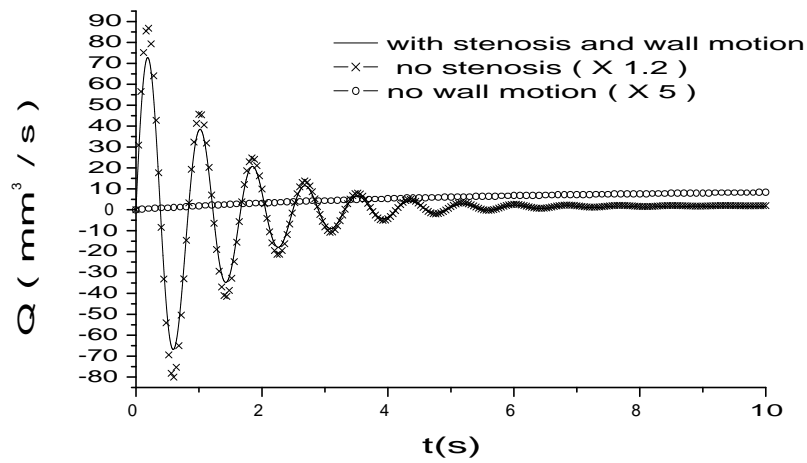


Figure 11: Variation of the flow rate with time at the offset of the stenosis.

One should note that the effect of constriction on the flow rate appears to be significant to some extent only in Figure 10 and the maximum effect of wall distensibility on the flow rate arises in Figure (8) relative to the rest of the results. The results of these figures possess a common feature that the flow rate curves become steady to some extent after expiry of the sixth cardiac cycle when the wall motion is taken into account.

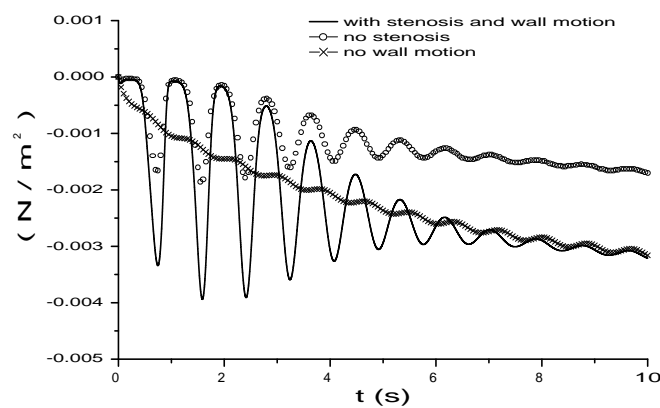


Figure 12: Variation of the wall shear stress at the parent aorta ($z = 6$ mm) with time.

Figure (12) records the behaviour of the time variant wall shear stress at the parent aorta at $z = 6\text{ mm}$ corresponding to its maximum constriction site. Two more curves are also plotted in this figure : (i) in the absence of any constriction and (ii) in the absence of wall motion as noted with distinguishable marks. It appears that the wall shear stress increases a little from zero at the onset of the first cardiac cycle during systole and diminishes largely during diastole followed by continuously increase and decrease depending upon the systolic and the diastolic phases of the next several cardiac cycles and eventually it becomes steady towards the end of the time advancement. Back flow does take place with the formation of two small separation zones during the first two cardiac cycles.

Almost similar feature is observed in the case of the absence of any constriction but with considerable deviation in magnitudes. One may note in this connection that the stress values get reduced considerably when the parent arterial constriction is completely disregarded. When the wall motion is withdrawn from the present system, the stress curve almost continuously declines without having any major fluctuations and hence one can estimate the influence of wall distensibility on the wall shear stress quantitatively right through the comparison of the relevant curves of the present figure.

Unlike the characteristics of the wall shear stress in the parent aorta, Figures (13)(14)(15)(16) represent the variations of the wall shear stress experienced by the daughter outer wall with time at various respective locations viz. (i) at the apex, (ii) at the onset of stenosis, (iii) at the maximum constriction site and (iv) at the offset of stenosis. All these figures also include the corresponding results by disregarding the presence of constriction and by ignoring the vessel wall distensibility. The stresses experienced by the daughter outer wall appear to be over hundred times more than those experienced by the parent wall.

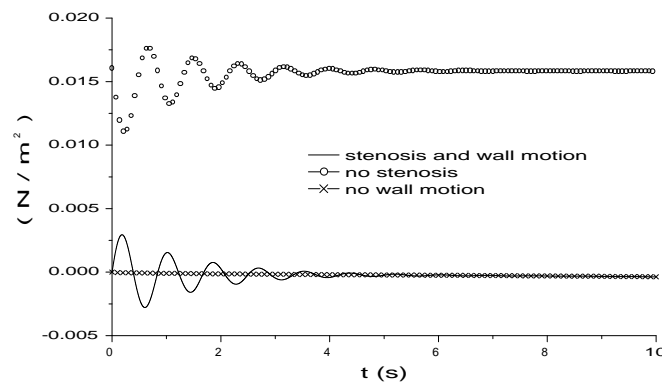


Figure 13: Variation of the outer wall shear stress at the apex with time.

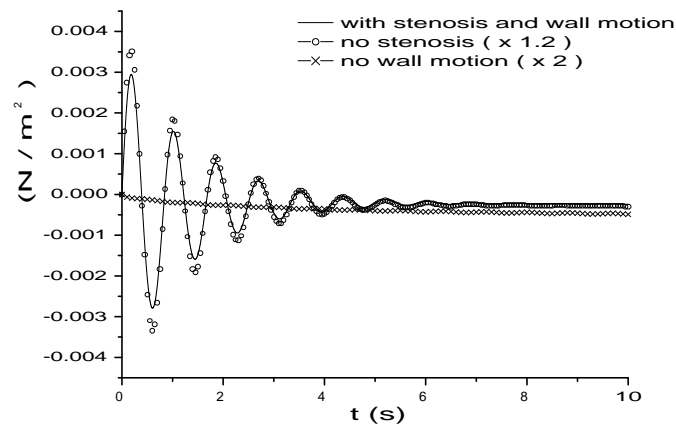


Figure 14: Variation of the outer wall shear stress at the onset of the stenosis with time.

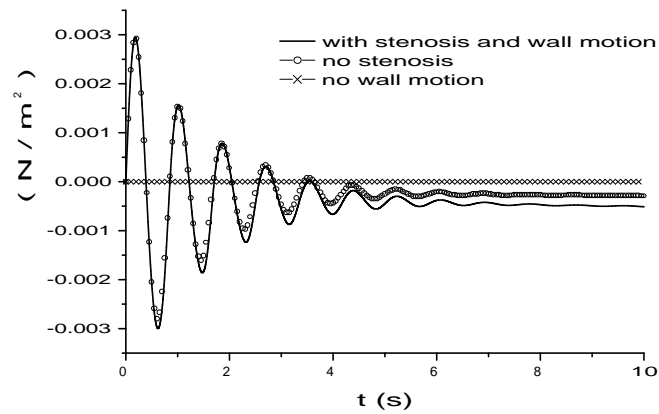


Figure 15: Variation of the outer wall shear stress at the maximum constriction site.

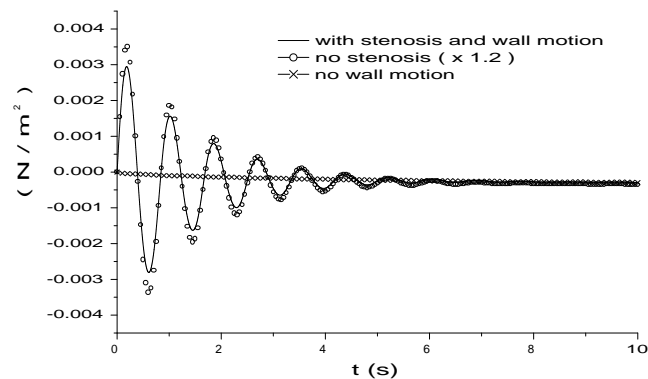


Figure 16: Variation of the outer wall shear stress at the offset of the stenosis with time.

The stress characterizes to have large fluctuations from positive to negative, negative to positive and so on towards the first few cardiac cycles and eventually the fluctuations with variable amplitudes gradually die out with large advancement of time. The stress curves become steady beyond $t = 6$ s where no further fluctuations are found to form. Such behaviour of stress includes back flow with the formation of several flow separation zones. The magnitudes of the stress get reduced considerably when one disregards the presence of constriction as also when the wall motion is withdrawn from the present system. It is worth while to mention that the sign of the wall shear stress becomes positive when the flow is forward and negative when the stream is reversed. It has been suggested that the change of shear stress direction or amplitude within a cardiac cycle may have some relevance to atherogenesis (cf. McDonald [23]). It has also been speculated by Fischer et al [24] that the increased collagen production resulting from the pulsatile wall stretch due to pulsatile pressure gradient may be an initiating event in vessel wall injury leading to atherogenesis. Thus the observations of the present results agree well with this hypothesis and perhaps it would help understanding the development of arterial diseases.

Finally, the concluding Figures (17)(18)(19) present the variations of the stress experienced by the daughter inner wall with time at three specific locations respectively — (i) at the onset of the constriction, (ii) at the maximum constriction site and (iii) at the offset of the stenosis. Unlike those of the outer daughter wall, the wall shear stress on the inner daughter wall appears to gain its magnitude quite higher for the entire time range considered here which becomes all time positive with several fluctuations towards the early period of a few cardiac cycles till time $t = 5$ s and then it remains almost steady for rest of the time. In the absence of the stenosis, the stress values are reduced significantly only in the stenotic region than at the onset and the offset of the stenosis.

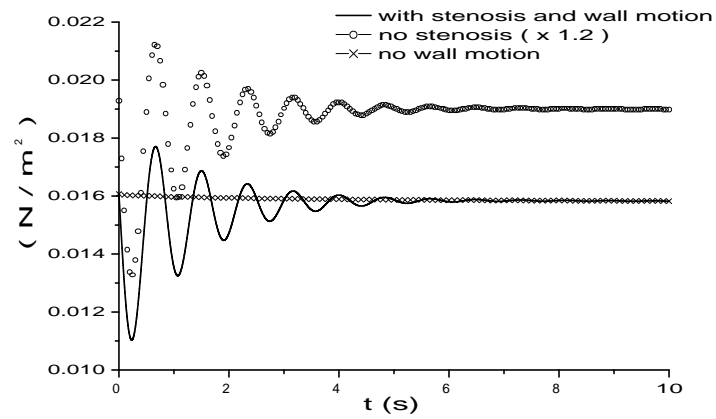


Figure 17: Variation of the inner wall shear stress with time at the onset of the constriction.

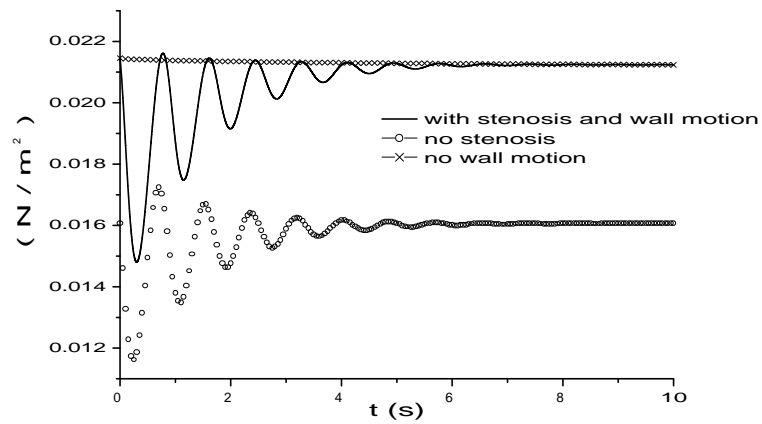


Figure 18: Variation of the inner wall shear stress at the maximum constricted site with time.

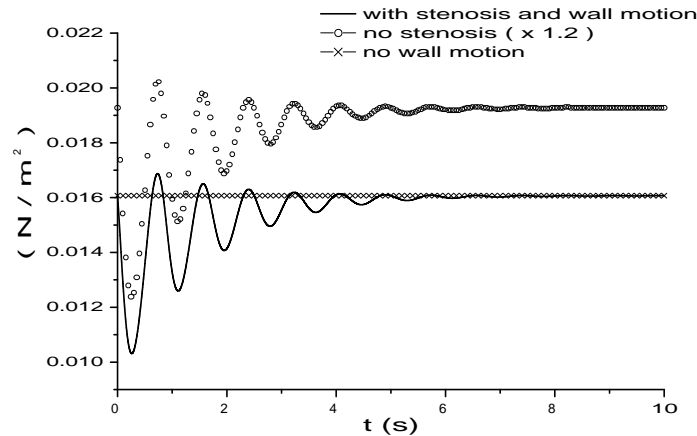


Figure 19: Variation of the inner wall shear stress at the offset of the constriction with time.

A considerable reduction of the stress values is also recorded when the wall motion is disregarded. The distensible bifurcation experiences shear stresses higher to some extent than those of a rigid bifurcation at both the inner and the outer wall of the branch artery. The inner wall shear stress does not show flow reversal and hence no flow separation zones are detected irrespective of the presence and the absence of the arterial constrictions and of the wall motion. In the present context, it may be worthwhile to mention that there have been two major hypotheses that relate to a possible hemodynamic role in atherogenesis – one is the low shear stress proposed by Caro et al [25] and the other is the high shear stress reported by Fry [2]. Both are equally important in the realm of bifurcated arterial flow phenomena and hence proper emphasis needs to be put on them so as to validate the applicability of the present model.

7. APPENDIX

The quantities $a_{i,j}^k$, $b_{i,j}^k$, $c_{i,j}^k$, $d_{i,j}^k$, $e_{i,j}^k$ and $f_{i,j}^k$ involved in the difference equation (5.1) have got their respective expressions given by

$$a_{i,j}^k = \xi_j \frac{\partial R_i^k}{\partial t} + \frac{\partial R_{2,i}^k}{\partial t} + \frac{\mu}{\rho(\xi_j R_i^k + R_{2,i}^k)},$$

$$b_{i,j}^k = -\frac{\mu}{\rho} \left[\frac{\partial^2 R_{2,i}^k}{\partial z^2} + \xi_j \frac{\partial^2 R_i^k}{\partial z^2} - \frac{2}{R_i^k} \frac{\partial R_i^k}{\partial z} \left(\xi_j \frac{\partial R_i^k}{\partial z} + \frac{\partial R_{2,i}^k}{\partial z} \right) \right],$$

$$c_{i,j}^k = -\frac{1}{(\xi_j R_i^k + R_{2,i}^k)} \left[R_{2,i}^k u_{i,1}^k + R_{1,i}^k \xi_j^2 (2 - \xi_j^2) \left(\alpha \frac{\partial R_{1,i}^k}{\partial t} - \frac{R_{2,i}^k}{R_{1,i}^k} u_{i,1}^k \right) \right],$$

$$d_{i,j}^k = \frac{1}{2\Delta\xi R_i^k} (w_{i,j+1}^k - w_{i,j-1}^k),$$

$$e_{i,j}^k = \frac{\mu}{\rho R_i^k (\Delta\xi)^2} \left[1 + \left(\xi_j \frac{\partial R_i^k}{\partial z} + \frac{\partial R_{2,i}^k}{\partial z} \right)^2 \right] (w_{i,j+1}^k - 2w_{i,j}^k + w_{i,j-1}^k),$$

and

$$f_{i,j}^k = \frac{\mu}{\rho(\Delta z)^2}(w_{i+1,j}^k - 2w_{i,j}^k + w_{i-1,j}^k) - \frac{w_{i,j}^k}{2(\Delta z)}(w_{i+1,j}^k - w_{i-1,j}^k).$$

REFERENCES

- [1] S. WOLF and N. T. WERTHESSEN, Dynamics of arterial flow, *Advances in Experimental Medicine and Biology*, **115**, (1979), p. 385, Plenum Press, New York.
- [2] D. L. FRY, Acute vascular endothelial changes associated with increased blood velocity gradients, *Circulation Res.* **22**, (1968) pp. 165-197.
- [3] M. R. ROACH and N. B. SMITH, Does high shear stress induced by blood flow lead to atherosclerosis ? *Perspect. Bio. Med.* **26**, (1983) 287.
- [4] C. K. ZARINS, D. P. GIDDENS, B. K. BHARADVAJ, V. S. SOTTIURAI and R. F. MABON, Carotid bifurcation atherosclerosis quantitative correlation of plaque localization with flow velocity profiles and wall shear stress. *Circulation Res.* **53**, (1983) pp. 502-514.
- [5] D. N. KU, D. P. GIDDENS, C. K. ZARINS and S. GLAGOV, Pulsatile flow and atherosclerosis in the human carotid bifurcation . *Atherosclerosis* **5**, (1985) pp. 293-302.
- [6] S. GLAGOV, C. ZARINS , D. P. GIDDENS, D. N. KU, Hemodynamics and atherosclerosis : insights and perspectives gained form studies of human arteries. *Arch. Pathol. Laboratory Med.* **112**, (1988) pp. 1018-1031.
- [7] M. H. FRIEDMAN, A biologically plausible model of thinning of arterial intima under shear. *Atherosclerosis* **9**, (1989) pp. 511-522.
- [8] Z. LOU and W. J. YANG , Biofluid dynamics at arterial bifurcations. *Critical Rev. Biomed. Engng.* **19**, (1992) pp. 455-493.
- [9] K. PERKTOLD, M. RESCH and H. FLORIAN , Pulsatile non-Newtonian flow characteristics in a three-dimensional human carotid artery bifurcation model. *Trans. ASME J. Biomech. Engng.* **113**, (1991) pp. 464-475.
- [10] K. PERKTOLD, R. O. PETER and R. GÜRTL, Computer simulation of flow phenomena in distensible arterial bifurcation models. In *Proc.(VI) Mediterranean Conference on Medical and Biological Engineering, MEDICON 92* (Edited by Bracale, M. and Denoth, F.)(1992) pp. 377-381, Area di Ricerca CNR-Pisa.
- [11] K. PERKTOLD and G. RAPPITSCH , Numerical analysis of arterial wall mechanics and local blood flow phenomena. In : *Advances in Bioengineering, ASME-BED-Vol. 26* (Edited by Tarbell, J. M.), (1993) pp. 127-131, ASME, New York.
- [12] S. CHAKRAVARTY, P. K. MANDAL and A. MANDAL, Mathematical model of pulsatile blood flow in a distensible arotic bifurcation subject to body accleration, *Int. J. Engng. Sci.* **38**, (2000) pp. 215-238.
- [13] M. KASHIHARA, K. MATSUMOTO and J. CERVOS-NAVARRO, Observations on carotid bifurcation, atherosclerosis in human cadavers, In: *Role of Blood Flow in Atherogenesis* (Edited by Yoshida , Y., Yamaguel, T. Caro, C. G., Glagov, S. and Nerem, R. M.) *Proc. Int. Symp.* **19** (1988), Springer-Verlag, Tokyo.
- [14] F. N. VAN DE VASSE, A. A. VAN STEENHOVEN, J. D. JANSSEN and R. S. RENEMAN, A two-dimension numerical analysis of unsteady flow in the carotid artery bifurcation, *Biorheology* **27**, (1990) pp. 163-189.
- [15] A. C. BURTON, *Physiology and Biophysics of the Circulation*, Year Book Medical Publisher, Chicago (1966).

- [16] J. R. WOMERSLEY, Oscillatory flow in arteries, the constrained elastic tube as a model of arterial flow and pulse transmission, *Phys. Med. Biol.* **2**, (1957) pp. 178-187.
- [17] S. C. LING and H. B. ATABEK, A nonlinear analysis of pulsatile flow in arteries, *J Fluid Mech.* **55**, (1972) pp. 493-511.
- [18] K. IMAEDA and F. O. GOODMAN, Analysis of nonlinear pulsatile blood flow in arteries, *J. Biomech.* **13**, (1980) pp. 1007-1022.
- [19] M. DESHPANDE, D. GIDDENS and R. MABON, Steady flow through modelled vascular stenosis, *J. Biomech.* **9**, (1976) pp. 165-174.
- [20] T. J. PEDLEY, *The Fluid Mechanics of Large Blood Vessels*, Cambridge University Press, Cambridge (1980).
- [21] W. R. MILNOR, *Haemodynamics*, Williams and Williams, Baltimore (1982).
- [22] K. PERKTOLD and G. RAPPITSCH, Computer simulation of local blood flow and vessel mechanics in a compliant carotid artery bifurcation model, *J. Biomech.* **28**, (1995) pp. 845-856.
- [23] D. A. McDONALD, *Blood Flow in Arteries*, 2nd ed., Edward Arnold, London (1974).
- [24] G. M. FISCHER, M. L. SWAIN, K. CHERIAN, Pulsatile distension and vascular collagen synthesis in the rabbit, *Blood Vessels* **17**, (1980) p. 215.
- [25] C. G. CARO, J. M. FITZ-GERALD, and R. C. SCHROTER, Atheroma and arterial wall shear : observations correlation, and proposal of a shear dependent mass transfer mechanism for atherogenesis, *Proc. R. Soc. Lond.* **B177**, (1971) p. 109.